Reduced cerebral vascularisation in experimental neuronopathic Gaucher disease

RUNNING TITLE

Reduced cerebral vascularisation in Gaucher disease

AUTHOR LIST

Nicholas J. C. Smith[1,2,3,*], Jennifer T. Saville[4], Maria Fuller[2,4] and Timothy M. Cox[3]

[1]Department of Neurology and Clinical Neurophysiology, Women's and Children's Health Network, Adelaide, South Australia, 5006, Australia.

[2]School of Medicine, University of Adelaide, Adelaide, South Australia 5005, Australia.

[3]Department of Medicine, University of Cambridge, Cambridge, CB20QQ, United Kingdom.

[4]Genetics and Molecular Pathology, SA Pathology at Women's and Children's Hospital, Adelaide, South Australia, Australia, 5006, Adelaide.

[*] Correspondence to: Nicholas J.C. Smith, Department of Paediatrics, University of Adelaide and Department of Neurology and Clinical Neurophysiology, Women's and Children's Hospital, 72 King William Rd, North Adelaide, South Australia, Australia, 5006. Phone: 61-8-8161-7308, Fax: 61-8-8161-6224. Email: n.smith@adelaide.edu.au

CONFLICT OF INTEREST STATEMENT

NJCS was supported by the NIHR Biomedical Research Centre (Metabolic theme) and the University of Cambridge, UK and has received travel support from the Children's Gaucher Research Fund. JS, TMC have no conflicts of interest to declare. MF…..

WORD COUNT 3915

Deleted: UK

Deleted: Cambridge

Deleted: [Metabolic] in the completion of this work

Deleted: s

Deleted: TMC……..¶

Formatted: Highlight

ABSTRACT

The glycosphingolipidosis Gaucher disease, in which a range of neurological manifestations occur, results from a deficiency of acid β-glucocerebrosidase, with subsequent accumulation of β-glucocerebroside, its upstream substrates and the unacylated congener, ß-glucosylsphingosine. However, the mechanisms by which end-organ dysfunction arise are poorly understood. Here we report strikingly diminished cerebral microvascular density in a murine model of disease and provide a detailed analysis of the accompanying cerebral glycosphingolipidome in these animals, with marked elevations of ß-glucosylsphingosine. Further in vitro studies confirm a concentration dependent impairment of endothelial cytokinesis upon exposure to quasi-pathological concentrations of ß-glucosylsphingosine. These findings support a premise for pathogenic disruption of cerebral angiogenesis as an end-organ effect, with potential for therapeutic modulation in neuronopathic Gaucher disease.

KEY WORDS

Gaucher; angiogenesis; ß-glucosylsphingosine; actin.

Deleted: ¶

INTRODUCTION

Disorders of glycosphingolipid metabolism, such as Gaucher disease, are important causes of inherited neurodegeneration. The heterogeneous glycosphingolipidosis, Gaucher disease, in which diverse neurological manifestations occur, is due to deficiency of acid β-glucocerebrosidase, which leads to impaired lysosomal recycling of glucosylceramide accompanied by accumulation its unacylated congener, ß-glucosylsphingosine.

While disordered glycosphingolipid homeostasis is a primary feature of Gaucher disease, the mechanisms by which end-organ dysfunction and injury arise, particularly in the brain, are little understood.

In the biochemically related glycosphingolipid disease, globoid-cell leukodystrophy, (Krabbe disease) marked disturbances of cerebral angiogenesis are reported [1,2]; these authors provided compelling evidence that implicates the pathological accumulation of the cognate lysolipid, ß-galactosylsphingosine in its neuropathogenesis [1-3]. The complexity of glycosphingolipid control in the formation of vascular networks by higher-order gangliosides is well recognised [4-6] and, given the perturbation of these molecules in Gaucher disease [7-11], the potential for consequent disruption of cerebral angiogenesis merits further exploration. Since the two lysosphingolipids, ß-galactosylsphingosine and ß-glucosylsphingosine are closely related molecules, known collectively as 'psychosine', a common mechanism might also explain the ontogeny of acute neuronopathic Gaucher disease. Other striking shared pathological features of these diseases include the presence of large multi-nucleate tissue macrophages - the eponymous Gaucher cell and globoid cell in Gaucher and Krabbe disease respectively. It is notable also that exposure of cultured human macrophage-like cells to psychosines arrests cytokinesis and induces a Gaucher-like cell phenotype [12,13].

Here we report strikingly diminished cerebral microvascular density in an authentic and genetically coherent model of acute neuronopathic Gaucher disease generated in mice [14]; we further provide a detailed analysis of the accompanying cerebral glycosphingolipidome of these animals. Experimental studies using cultured primary human umbilical vein endothelial cells showed concentration-dependent impairment of

endothelial cytokinesis after exposure to quasi-pathological concentrations of ß-glucosylsphingosine.

In summary, we provide experimental evidence that the pathological glycosphingolipids which accumulate specifically in Gaucher disease, markedly disrupt cerebral microvasculature in a context that is likely to contribute materially to the severe neurological manifestations of this glycosphinglipidosis. Since several advanced molecular therapies are in late-stage development for neuronopathic Gaucher disease, we contend that due weight should be paid to a relationship between our findings and a putative effect of Gaucher disease on angiogenesis and formation of the fully ramified microvascular network in the mature brain.

MATERIALS AND METHODS

Deleted:

Animal model

The conditional mouse model of acute neurological Gaucher disease (nGD) (K-14Cre-positive *gba*$^{lnl/lnl}$) employed in these experiments is well-characterised, and develops an acute neuronopathic phenotype resembling the severe human disease subtype, type 2 Gaucher disease, 14]. Experimental homozygotes at mutant *gba* locus and paired, gender-matched, littermate control animals were harvested on post-natal day (PND) 14 for analysis. This work was performed under United Kingdom Home Office licence (PPL 80/2109) in accordance with the Animals (Scientific Procedures) Act 1986 and regulated by the institutional animal welfare and scientific procedure guidelines.

Quantification of neocortical and thalamic cerebral microvasculature vessel length volume density

Animals were terminally anaesthetised by intraperitoneal injection of 20% sodium pentobarbital, exsanguinated and transcardially perfused under manual pressure via 60 mL Luer-lock syringe; first-phase perfusion was performed with India ink, diluted in PBS at a dilution ratio of ink:PBS = 1:1, followed by a second perfusion with India ink diluted in 4% paraformaldehyde in PBS, at a dilution ratio of ink:paraformaldehyde = 0.5:1. Whole brains were removed and post-fixed by immersion in 4% $^{w/v}$ paraformaldehyde for 72 hours. Serial coronal sections (30µm) were cut, slide mounted and counter stained (cresyl violet 0.5%) for analysis.

Quantification of vessel length-volume density (L_{vd}) was carried out in preselected anatomical regions of interest: i) the neocortex and ii) the thalamus. Non-contiguous sections at 120µm intervals in the coronal axis were selected at three sampling regions from the neocortex and two regions within the thalamus, over bilateral hemispheres to yield a total of 18 (neocortical) and 12 (thalamic) sampling fields per animal. Selected fields were imaged by bright field microscopy at 4x objective magnification; digital images were captured for off-line analysis using ImageJ software (*U. S. National Institutes of Health, Bethesda, Maryland, USA*, http://imagej.nih.gov/ij/, 1997-2012). These analyses were conducted by an operator blinded in respect of the experimental group from which the tissue was obtained. Selected fields were overlaid with a gridded sampling probe (300 x 300µm per frame) and total vessel length was averaged over 3 frames per field, selected by systematic random sampling. Measurements were conducted in 2-dimensional reference using the ImageJ segmental tracing tool; aggregate

measurements were expressed as an average linear density per μm^3 (accounting for the 30 μm depth of the tissue section). Difference in mean values was compared by two-tailed Student's t-test ($\alpha = 0.05$) with assumed homoscedastic variance.

Quantification of multinucleated cells in ß-glucosylsphingosine-treated human umbilical vein endothelial cell monolayers

Primary human umbilical vein endothelial cells (HUVECs) (*Health Protection Agency*) were cultured in EBM-2 basal medium + EGM™-2MV BulletKit™ (*Lonza*). All experiments utilised asynchronous primary cultures, harvested from a common passage. Untreated cells were plated on borosilicate coverslips in 6-well plates, at a uniform density of 0.5×10^5 cells per well for 24 hours; at which point, exchange with ß-glucosylsphingosine (D-Glucosyl-β1-1'-D-erythro-Sphingosine) (*Avanti Polar Lipids*) containing medium at 0μM (vehicle only control), 5μM and 10μM concentrations was undertaken. All treatments were conducted in triplicate and 3 experimental replicates were carried out on separate occasions. Monolayers were harvested at 24 and 48 hours' post treatment and fixed in 4% paraformaldehyde for analysis. Monolayers were stained with tetramethylrhodamine isothiocyanate conjugated phalloidin (*Invitrogen*), at a concentration of 6.25μg/ml for 45 minutes at room temperature and mounted with anti-fade mounting agent containing 4',6-diamidino-2-phenylindole (Prolong Gold®). Laser scanning confocal microscopy (*Leica SP-5 LSCM*) was performed at 10x objective magnification for quantification of percentage multinucleated cells per unit area. Randomly selected images were digitally captured for off-line analysis, conducted blind to treatment effect; images were overlaid with a 1550μm x 1550μm sampling probe and count strategies employed the stereological principle of the 'dead-side' rule, with

exclusion of cells falling within the sampling frame if intersected by either of the 'excluded' perpendicular borders. Mononucleated, binucleated and multinucleated (≥ 3 nuclei) cells were quantified as a percentage of total cells within the sampling frame. In each experiment a total of three sampling frames were analyzed per treatment concentration. One-way analysis of variance ($\alpha = 0.05$) with a Bonferroni post hoc analysis was employed for comparison of percentage count by treatment concentration.

Quantitative analysis of monolayer wound closure in glucosylsphingosine treated human umbilical vein endothelial cell monolayers

Asynchronous HUVEC cultures were used for wound healing assays. After obtaining these cells as described above, monolayers were plated at uniform density and grown to confluence in 24-well tissue culture plates, pre-marked with scored reference grids. Linear wounds were manually inflicted along the diameter of the well using a sterile p20 pipette tip, cellular debris removed and fresh culture medium with containing serially increasing concentrations of ß-glucosylsphingosine applied at 0µM (vehicle only control), 0.6µM, 1.25µM, 2.5µM, 5µM, 10µM and 15µM. A minimum of three replicate wound assays were performed per experiment. Wounds were serially imaged at 0 hours, 8 hours, 20 hours, and 40 hours, to the point of wound closure. Parallel experiments were carried out after inhibiting endogenous β-glucocerebrosidase by exposure to the irreversible and selective suicide inhibitor, cyclophellitol (2.5µg /ml), effecting near total inhibition of acid β-glucocerebrosidase activity (data not shown). Serial measurements of wound width (relative to fixed reference markings) were averaged over three measurements per time point. Each treatment was carried out in triplicate and expressed as mean percentage wound closure; complete closure was assigned to the a ceiling effect

at the first time point achieved. Statistical comparison of mean percentage closure with respect to ß-glucosylsphingosine concentration was assessed by 2-way analysis of variance ($\alpha = 0.05$) using the Bonferroni post hoc correction and assuming homoscedastic variance.

Lipidomic analysis of brain regions

Animals were terminally anaesthetised (as previously described), exsanguinated and their whole brains dissected from the skull; the neocortex and subcortex were anatomically dissected, snap frozen in liquid nitrogen and stored at -80ºC for lipid analysis. Each brain region was resuspended in 0.02 M Tris (pH 7) containing 0.5 M NaCl and 0.1% Nonidet P-40 (10X volume per weight) and homogenised on ice in a 4.5 mL glass Dounce homogeniser. Total protein was determined by the method of Lowry et al. (1957) and 0.01 mL of 5 µg/µL and 10 µg/µL was extracted for sphingolipids and gangliosides respectively, with the addition of 0.2 mL of $CHCl_3$:CH_3OH (2:1) containing 5 pmol of dihydroceramide (dhCer) d18:0/8:0 {*N*-octanoyl-D-*erythro*-sphinganine}, sphingomyelin (SM) d18:1/12:0 {*N*-lauroyl-D-*erythro*-sphingosylphosphorylcholine}, 10 pmol of ceramide (Cer) d18:1/17:0 {*N*-heptadecanoyl-D-*erythro*-sphingosine}, dihexosylceramide (DHC) d18:1/16:0 (d_3) {*N*-palmitoyl-d_3-lactosylceramide}, monohexosylceramide (MHC) d18:1/16:0 (d_3) {*N*-palmitoyl-d_3-glucopsychosine} trihexosylceramide (THC) d18:1/17:0 {*N*-heptadecanoyl ceramide trihexoside}, G_{M1} d18:1/18:0 (*d3*) {(*N-omega* C*d3*-octadecanoyl monosialoganglioside G_{M1} d18:1/18:0 (ammonium salt)} and 1 nmol of cholesterol (*d7*) as internal standards (Standards purchased from Avanti Polar Lipids, with the exception of DHC, MHC, THC and G_{M1} from Matreya LLC). After brief agitation in Vortex mixer, samples were mixed on a

rotary mixer for 10 mins, sonicated in a water bath for 30 mins and then allowed to stand at room temperature for 20 mins. The protein was sedimented by centrifugation at 13,000g for 10 mins at RT, the supernatant removed and dried under a gentle stream of nitrogen at 40ºC. Samples were stored at -20 ºC until LC-ESI-MS/MS analysis.

The lipid extract was reconstituted in 0.1 mL of CH_3OH containing 10 mM NH_4COOH and for all lipids, except gangliosides, 1 µl was injected onto a Zorbax Eclipse C18, 2.1 mm x 50 mm column maintained at 40ºC (CTO-30A oven) using a Shimadzu Nexera *x*2 SIL-30AC autosampler maintained at 16ºC configured with LC 30 AD pumps. A 1290 inline filter containing a 0.3 µm frit was placed in front of the column. Solvent A was 60% H_2O, 40% CH_3CN containing 10 mM NH_4COOH and solvent B was 90% $(CH_3)_2CHOH$, 10% CH_3CN containing 10 mM NH_4COOH. At injection, mobile phase conditions were 90% solvent A and 10% solvent B, which was linearly ramped to 50% by 2 mins and then to 100% solvent B at 8.0 mins. This was held for 0.5 mins followed by a return to 90% solvent A at 9 mins, which was equilibrated for 1 min prior to the next injection. The flow rate was 0.4 mL/min.

For the first minute column flow was diverted to waste and then directly into the electrospray source (ES 5500 V) of an AB SCIEX 6500 QTrap triple quadrupole tandem mass spectrometer with an ion source temperature of 250ºC. Nitrogen was used for curtain gas, 25 units; collision gas set at medium; nebuliser gas 1, 20 units and auxillary gas 2, 45 units. Individual species of dhCer, Cer, DHC, MHC, THC and sulphatides, as well as the single species, glucosylsphingosine were quantified using scheduled multiple reaction monitoring (MRM) in positive ion mode (see Supplementary Table 1). Concentrations of each molecular species were calculated by relating the peak areas of

each species to the peak area of the corresponding internal standard using MultiQuant 3.0.2 software. For sulphatides and glucosylsphingosine, THC d18:1/17:0 and DHC d18:1/16:0 d_3, respectively, were used.

Individual species of gangliosides were quantified in a separate acquisition method in negative ion mode (ES -4500) with a less precipitous LC gradient. Mobile phase A and B were as described above except 0.05% NH_4OH replaced NH_4COOH to ensure the larger gangliosides (MW > 1000) could be quantified as doubly charged ions. At injection, mobile phase conditions were 90% solvent A and 10% solvent B, which was linearly ramped to 30% B by 5 mins, 60 % B by 8 mins and then to 100% B at 10.5 mins. This was held for 0.5 mins followed by a return to 10% B at 11 mins, which was equilibrated for 1 min prior to the next injection. Individual species of gangliosides were quantified using non-scheduled MRM and concentrations were calculated by relating the peak areas of each species to the peak area of G_{M1} 18:1/18:0 (*d3*) using MultiQuant 3.0.2 software.

Results are presented as the mean ± SEM with four nGD and four WT mice each assayed in triplicate. Differences between nGD and WT were analysed for significance using a two-tailed Student's *t*-test following an F-test for homoscedastic variance. Pearson's correlation coefficients between individual lipid species and the three brain regions were also determined using SPSS version 15.0 for Windows statistics software.

Deleted: ¶

RESULTS

Quantification of neocortical and thalamic cerebral microvasculature vessel length volume density

Matched disease (n=3) and control (n=3) animals were included for quantification of vessel length volume density (L_{vd}) within the neocortex and thalamus (cerebellar vascular density was not assessed). Regional analysis revealed a statistically significant reduction in mean L_{vd} within both the neocortex ($p = 0.0220$) and thalamus ($p = 0.0222$) of diseased relative to age and gender matched control animals; a trend that proved consistent within individual animals [Figure 1]. Mean neocortical L_{vd} (± SEM) measured $5.44 \pm 0.12 \times 10^{-4}$ $\mu m/\mu m^3$ and $4.36 \pm 0.27 \times 10^{-4}$ $\mu m/\mu m^3$ and mean thalamic L_{vd} measured $5.26 \pm 0.23 \times 10^{-4}$ $\mu m/\mu m^3$ and $4.13 \pm 0.21 \times 10^{-4}$ $\mu m/\mu m^3$ in control and diseased cohorts respectively. No significant difference was noted between subregions within each group.

Analysis of multinucleated cells in ß-glucosylsphingosine-treated human umbilical vein endothelial cell monolayers

Quantitative analysis of percentage multinucleate cell count, relative to glucosylsphingosine at quasi-pathological treatment concentrations was undertaken in human umbilical vein endothelial cell monolayers (HUVEC monolayers); three replicate experiments were performed, with analysis at 24 hour and 48 hour culture duration [Supplementary figure 1]. Mean percentage cell counts demonstrated increased binucleated ($p = 0.0416$) and multinucleated ($p = 0.0281$) percentages of total cell count in 5µM and 10µM treated monolayers, relative to vehicle only controls; post hoc Bonferroni analysis did not demonstrate individual comparator significance for binucleated percentage counts, while multinucleated cell percentages were significantly

greater at 5µM relative to untreated monolayers. This trend was reinforced at 48 hour analysis, with both binucleated ($p = 0.0008$) and multinucleated ($p = 0.0040$) cell percentages significantly increased following 5µM and 10µM glucosylsphingosine treatment; in both cases Bonferroni analysis confirmed significant increases relative to untreated monolayers, although increased effect with doubling of concentration (5µM vs 10µM) was not observed.

Quantitative analysis of monolayer wound closure in ß-glucosylsphingosine- and cyclophellitol-treated human umbilical vein endothelial cell monolayers

Wound healing assays (n=6) demonstrated a statistically significant reduction in mean percentage wound closure, relative to treatment concentration ($P_{interaction} = 0.0194$; $P_{GlcSph\ concentration} < 0.0001$; $P_{time} < 0.0001$). Post-hoc Bonferroni comparison confirmed significant effects for treatment concentrations ≥ 1.25µM glucosylsphingosine treatment (i.e. ≥ 1.25µM) at the 8 hour time point and from 10µM concentration for the remaining time points – reflecting ceiling wound closure of HUVEC monolayers in the majority of replicate experiments prior to the 20 hour time point. [Supplementary figure 2a]. Replicate experiments (n=3) utilizing monolayers pretreated with the irreversible β-glucocerebrosidase inhibitor, cyclophellitol, demonstrated treatment effects congruent with enzyme replete cultures; concentration dependent delays in mean percentage wound closure were recorded in ß-glucosylsphingosine-treated monolayers (n=3) ($P_{interaction} < 0.0001$; $P_{GlcSph\ concentration} < 0.0001$; $P_{time} < 0.0001$). As expected, greater sensitivity to exogenous ß-glucosylsphingosine was apparent when post-hoc Bonferonni analysis was carried out, with significant retardation of wound closure upon application of 0.6µM ß-

glucosylsphingosine (the lowest treatment concentration applied) compared to 1.25μM retardation in uninhibited cultures [Supplementary figure 2b].

Regional brain lipidomic analysis

Beta-glucosylsphingosine and total monohexosylceramide (MHC) (sum of seven individual species inclusive of ß-glucosylceramide) elevation was non-discriminatory, but concentrations of these compounds were significantly elevated in the cortex and sub-cortex of mice with neuronopathic Gaucher disease [Figure 2]. With the exception of the two longest acyl chain species, 24:0 and 24:1, that remained unchanged [Supplementary figure 3], the concentrations of most of the individual monohexosylceraminde species were also elevated. For dihexosylceramides (DHC) - the sphingolipid upstream of monohexosylceramide in the catabolic pathway- the distribution differed with the longer acyl chain species, 22:0, 24:0 and 24:1 significantly elevated in the experimental murine brain; in contrast, the shorter acyl chain derivatives, 16:0 and 20:0, were unchanged in the brain tissue from mutant animals. DHC 18:0 co-eluted with sulphatide 24:1 and could not be quantified. Trihexosylceramide was not detectable in brain tissue from either wild type or homozygous mutant mice with neuronopathic Gaucher disease.

Of the higher-order gangliosides, a-series species G_{M3}, G_{M2} and $G_{M1,}$ were all elevated in brain tissue from the homozygous mutant mice. Individual acyl chains of each species correlated (Pearson coefficient >0.7), with d18:1/18:0 as the most prominent isoform. G_{M1} ganglioside proved to be the most abundant, and was present at 80-fold the concentrations of G_{M2} and G_{M3} [Figure 3]. The more complex a-series ganglioside, G_{D1a}, was relatively conserved between the subregions of wild type and mutant mouse brain tissues, with only the longer chain 22:0 species ubiquitously elevated [Figure 4]. Of the

b-series, G_{D3} was more abundant than G_{D2} but all isoforms of both were significantly elevated in both subregions in the brain tissue of the homozygous mutant animals [Figure 5].

DISCUSSION

Here we report a marked reduction in the cerebral microvasculature volume density (L_{vd}) in a murine model of neuronopathic Gaucher disease. The determinations represent total vessel length per cubic micron of tissue and avoid technical bias introduced by the use of differing reference volumes [15]. While differences in vascular perfusion and luminal patency must be considered, the observed trend in vascular volume proved to be consistent in all the mutant diseased animals studied. The methodology employed here delineates functional angioarchitecture (vascular perfusion at the point of analysis) and it is noteworthy that our results concord with observations reported by Belleri and colleaguesin the cognate sphingolipidosis, Krabbe disease, where quantification of vascular density employed immunolabelling of vessel endothelium [1, 3]. Indeed, detailed studies in the homozygous (*galc* -/-) twitcher mouse model of Krabbe disease revealed intact spatial distribution of neocortical microvasculature, with a homogeneous reduction in total vascular length and increased vessel fragmentation. In their latter publications, these authors reported increased intussusceptive angiogenesis with upregulated expression of genes integral to this process, suggesting a primary impairment of sprouting angiogenesis (a process dependent upon endothelial cytokinesis and cellular migration), with compensatory, inflammatory driven, intussusceptive vascularisation; attributing this to the accumulation of the psychosine, ß-galactosylsphingosine, a substrate with recognised anti-angiogenic properties [3,16]. Our results extend this

premise, to the closely related ß-glucosylsphingosine molecule, which accumulates in Gaucher disesase, and is a diastereoisomer form of psychosine, ß-galactosysphingosine. We identified a concentration-dependent impairment of endothelial cytokinesis and migration upon exposure to pathophysiological concentrations of the substrate, and compatible with the disruption of endothelial actin stress fibres also reported on treatment with micromolar concentrations of ß-glucosylsphingosine by Belleri and colleagues [1].

While a class effect, amongst these related unacylated monohexosylceramide molecules is highly probable (and indeed in part revealed by the experiments of Belleri *et al*), the unitary molecular pathways by which these compounds influence angiogenesis are unclear; ß-glucosylsphingosine and ß-galactosylsphingosine stimulate activity of phospholipase A2 (PLA2), which in turn generates anti-angiogenic lysophosphatidylcholine [5,17-19]. Additionally, these substrates are known to inhibit thrombin generation, itself a pro-angiogenic mediator [5]. Indeed, several lysosphingolipids, including pro-angiogenic sphingosine-1-phosphate, serve identified roles in both developmental and pathological angiogenesis [5,20-25]. In the case of sphingosine-1-phosphate, as a ligand of the lysophospholipid G-protein coupled receptor subfamily – activation of which induces endothelial cell migration and capillary tube formation [26-30].

The first clear description of the effect of psychosine on cytokinesis was reported by Kanazawa et al [12], with the T-cell death-associated gene 8 (TDAG8), a G-protein-coupled receptor, implicated as a potential ligand by overexpression studies in psychosine-mediated inhibition of cytokinesis [13]. A member of the dual proton-sensing ovarian cancer G-protein-coupled receptor (OGR1) subfamily – binding of which has

been implicated in the dysregulation of actin dynamics [13,24,31-35]. Indeed, it is of interest that knock-out models of the GPR4 receptor, another member of this subfamily, demonstrate formative abnormalities of vascular networks [36,37]. However, latterly, TDAG8 has been reported unequivocally dispensable for psychosine-induced formation of multinucleated cells [38] and alternate mechanisms have been implicated, with inhibition of cytokinesis by ß-galactosylsphingosine associated with clustering of sphingomyelin at the cell surface, as well as impaired generation of phosphatidylinositol 4,5-bisphosphate at the cleavage furrow in cultured cells [39]; since both of these steps are critical accompaniments of cytokinesis, another cytological explanation for the observed multiploidy is available.

Dyshomeostasis of the complex gangliosides in Gaucher disease has been long-studied [11,40,41]: we confirm ubiquitous accumulation of the a-series of gangliosides, G_{M1}, G_{M2} and G_{M3}, with G_{M1} the most abundant, present at 80-fold the concentration of G_{M2} and G_{M3}. Accumulation of the b-series gangliosides, G_{D2} and G_{D3}, was also evident.

While a concentration-dependent effect can be suggested for the anti-angiogenic action of glucosylsphingosine, this same relationship does not hold true for the complex gangliosides where pro-angiogenic compounds G_{M1}, G_{M2}, G_{D1a} and G_{D3} [4,42-46] dominate by volume over gangliosides with suggested anti-angiogenic actions, most particularly G_{M3} [6,42,47,48]. This might be explained by a dominant pathogenic effect of glucosylsphingosine – in line with the long held, though incomplete, ‘psychosine hypothesis’ of pathogenicity [49]. However, the possibility that wider disruption of lipid homeostasis contributes to the phenomena of disordered angiogenesis cannot be dismissed, with perturbation of lipid signalling, lipid raft clustering and raft composition

implicated [43,50]. The latter impacting membrane targeting of proteins integral to the regulation of angiogenesis, such as the urokinase plasminogen activator receptor (uPAR), a pro-angiogenic mediator, which is preferentially recruited to membrane regions enriched with the pro-angiogenic G_{M1} ganglioside and depleted of anti-angiogenic GM_3 [51]. Increased G_{M3}, relative to total and specific gangliosides is also recognised to impair angiogenesis [4,42,48,52-54], while G_{M3} inhibition of endothelial cell proliferation, migration and new vessel formation can be counteracted by the presence of pro-angiogenic gangliosides including G_{T1b}, G_{D1a} and G_{D3} [4,42,48]. It is notable that in our analyses, the relative concentrations of pro-angiogenic sphingolipids dominate over identified anti-angiogenic compounds, raising the possibility of a hierarchy of lipid mediated angiogenic regulation, with the pathogenic actions of glucosylsphingosine predominant. Indeed, analysis of relative ganglioside ratios within the neuronopathic Gaucher model herein, found little difference between the ratios of reportedly pro-angiogenic gangliosides and anti-angiogenic G_{M3} [Table 1]; the exception being a relative increase in G_{M2}:G_{M3} in the diseased state, a finding which is superficially incongruent with the premise of G_{M2} as a pro-angiogenic compound, but likely reflects the complex contribution of sphingolipids in angiogenic regulation. Tissue specific effects upon angiogenesis might also be considered; by example, G_{D3} is considered pro-angiogenic within the cornea and central nervous system [52,55], while reportedly attenuating vessel formation within a pancreatic tumour model [56].

CONCLUSION:

While perturbations in cerebral angiogenesis does not provide a complete explanation for neurodegeneration in Gaucher disease, our reported observations and those in the biochemically related Krabbe disease, support contribution of such a mechanism, perhaps in part, the result of disturbed actin dynamics [12,13], a premise that warrants further attention, with potential for therapeutic modulation of vasculogenesis in these diseases.

REFERENCES

1. Belleri M, Ronca R, Coltrini D, et al. Inhibition of angiogenesis by β-galactosylceramidase deficiency in globoid cell leukodystrophy. *Brain.* 2013;**136**:2859-75.
2. Zizioli D, Guarienti M, Tobia C, Gariano G, Borsani G, Bresciani R, Ronca R, Giacopuzzi E, Preti A, Gaudenzi G, Belleri M, Di Salle E, Fabrias G, Casas J, Ribatti D, Monti E, Presta M. Molecular cloning and knockdown of galactocerebrosidase in zebrafish: new insights into the pathogenesis of Krabbe's disease. *Biochim Biophys Acta.* 2014;**1842**:665-75.
3. Giacomini A, Ackermann M, Belleri M, et al. Brain angioarchitecture and intussusceptive microvascular growth in a murine model of Krabbe disease. *Angiogenesis*. 2015;**18**:499-510.
4. Manfredi M, Lim S, Claffey K, et al. Gangliosides influence angiogenesis in an experimental mouse brain tumor. *Cancer Res.* 1999;**59**:5392-7.
5. Dyatlovitskaya EV. The role of lysosphingolipids in the regulation of biological processes. *Biochemistry (Mosc).* 2007;**72**:596-602.
6. Liu Y, Wondimu A, Yan S, et al. Tumor gangliosides accelerate murine tumor angiogenesis. *Angiogenesis.* 2014;**17**:563-71.
7. Nilsson O, Svennerholm L. Accumulation of glucosylceramide and glucosylsphingosine (psychosine) in cerebrum and cerebellum in infantile and juvenile Gaucher disease. *J Neurochem*. 1982;**39**:709-718.
8. Kaye E, Ullman M, Wilson E, et al. Type 2 and type3 Gaucher's disease: a morphologic and biochemical study. *Ann Neurol*. 1986;**20**:223-230.

9. Orvisky E, Park J, La Marca M, et al. Glucosylsphingosine accumulation in tissues from patients with Gaucher disease: correlation with phenotype and genotype. *Mol Genet Metab.* 2002;**76**:262-270.
10. Farfel-Becker T, Vitner E, Kelly S, et al. Neuronal accumulation of glucosylceramide in a mouse model of neuronopathic Gaucher disease leads to neurodegeneration. *Hum. Mol. Genet.* 2014;**23**:843-854.
11. Karageorgos L, Hein L, Rozaklis T, et al. Glycosphingolipid analysis in a naturally occurring ovine model of acute neuronopathic Gaucher disease. *Neurobiol Dis.* 2016;**91**:143-54.
12. Kanazawa T, Nakamura S, Momoi M, et al. Inhibition of Cytokinesis by a Lipid Metabolite, Psychosine. *J Cell Biol.* 2000;**149**:943-950.
13. Im D, Heise CE, Nguyen T, et al. Identification of a Molecular Target of Psychosine and Its Role in Globoid Cell Formation. *J Cell Biol*. 2001;**153**:429-434.
14. Enquist I, Lo Bianco C, Ooka A, et al. Murine models of acute neuronopathic Gaucher disease. *Proc Natl Acad Sci U S A.* 2007;**104**:17483-8.
15. Mayhewaf T, Huppertz B, Kaufmann P, et al. The 'Reference Trap' Revisited: Examples of the Dangers in Using Ratios to Describe Fetoplacental Angiogenesis and Trophoblast Turnover. *Placenta.* 2003;**24**:1-7.
16. Belleri M, Presta M. Endothelial Cell Dysfunction in Globoid Cell Leukodystrophy. *J Neurosci Res.* 2016;**94**:1359-67.
17. Rikitake Y, Kawashima S, Yamashita T, et al. Lysophosphatidylcholine inhibits endothelial cell migration and proliferation via inhibition of the extracellular

signal-regulated kinase pathway. *Arterioscler Thromb Vasc Biol*. 2000;**20**:1006-1012.

18. Schueler U, Kolter T, Kaneski C, et al. Toxicity of glucosylsphingosine (glucopsychosine) to cultured neuronal cells: a model system for assessing neuronal damage in Gaucher disease type 2 and 3. *Neurobiol Dis.* 2003;**14**:595-601.
19. Schilling T, Lehmann F, Rückert B, et al. Physiological mechanisms of lysophosphatidylcholine-induced de-ramification of murine microglia. *J Physiol*. 2004;**557**:105–120.
20. Dyatlovitskaya EV, Kandyba AG. Sphingolipids in tumor metastases and angiogenesis. *Biochemistry (Mosc).* 2006;**71**:347-353.
21. Chatterjee S, Kolmakova A, Rajesh M. Regulation of lactosylceramide synthase (glucosylceramide beta1-->4 galactosyltransferase); implication as a drug target. *Curr Drug Targets.* 2008;**9**:272-281.
22. Saddoughi SA, Song P, Ogretmen B. Roles of bioactive sphingolipids in cancer biology and therapeutics. *Subcell Biochem.* 2008;**49**:413-440.
23. Kolmakova A, Rajesh M, Zang D, et al. VEGF recruits lactosylceramide to induce endothelial cell adhesion molecule expression and angiogenesis in vitro and in vivo. *Glycoconj J*. 2009;**26**:547-558.
24. Mochizuki N. Vascular integrity mediated by vascular endothelial cadherin and regulated by sphingosine 1-phosphate and angiopoietin-1. *Circ J*. 2009;**73**:2183-2191.

25. Loh KC, Baldwin D, Saba JD. Sphingolipid signaling and hematopoietic malignancies: to the rheostat and beyond. *Anticancer Agents Med Chem*. 2011;**11**:782-793.
26. Hia T, Lee MJ, Ancellin N, et al. Sphingosine-1-phosphate signaling via the EDG-1 family of G-protein-coupled receptors. *Ann N Y Acad Sci.* 2000;**905**:16-24.
27. Spiegel S. Sphingosine 1-phosphate: a ligand for the EDG-1 family of G-protein-coupled receptors. *Ann N Y Acad Sci.* 2000;**905**:54-60.
28. Oskouian B, Saba J. Sphingosine-1-phosphate metabolism and intestinal tumorigenesis: lipid signaling strikes again. *Cell Cycle.* 2007;**6**:522-527.
29. Hinkovska-Galcheva V, VanWay SM, Shanley TP, Kunkel RG. The role of sphingosine-1-phosphate and ceramide-1-phosphate in calcium homeostasis. *Curr Opin Investig Drugs.* 2008;**9**:1192-1205.
30. Limaye V. The role of sphingosine kinase and sphingosine-1-phosphate in the regulation of endothelial cell biology. *Endothelium.* 2008;**15**:101-112.
31. Okajima F, Kondo Y. Pertussis toxin inhibits phospholipase C activation and Ca2+ mobilization by sphingosylphosphorylcholine and galactosylsphingosine in HL60 leukemia cells. Implications of GTP-binding protein-coupled receptors for lysosphingolipids. *J Biol Chem.* 1995;**270**:26332-26340
32. Mitchison TJ. Psychosine, cytokinesis, and orphan receptors. Unexpected connections. *J Cell Biol.* 2001;**153**:1-3.
33. Gräler M, Goetzl E. Lysophospholipids and their G protein-coupled receptors in inflammation and immunity. *Biochim Biophys Acta*. 2002;**1582**:168-174.

34. Wang JQ, Kon J, Mogi C, et al. TDAG8 is a proton-sensing and psychosine-sensitive G-protein-coupled receptor. *J Biol Chem.* 2004;**279**:45626-45633.
35. Ishii S, Kihara Y, Shimizu T. Identification of T cell death-associated gene 8 (TDAG8) as a novel acid sensing G-protein-coupled receptor. *J. Biol. Chem*. 2005;**280**:9083-9087
36. Yang LV, Radu CG, Roy M, et al. Vascular abnormalities in mice deficient for the G protein-coupled receptor GPR4 that functions as a pH sensor. *Mol Cell Biol*. 2007;**27**:1334-1347.
37. Liu J, Komachi M, Tomura H, et al. Ovarian cancer G protein-coupled receptor 1-dependent and -independent vascular actions to acidic pH in human aortic smooth muscle cells. *Am J Physiol Heart Circ Physiol*. 2010;**299**:731-742.
38. Radu C, Cheng D, Nijagal A, et al. Normal immune development and glucocorticoid-induced thymocyte apoptosis in mice deficient for the T-cell death-associated gene 8 receptor. Mol Cell Biol. 2006;**26**:668-77.
39. Watanabe H, Okahara K, Naito-Matsui Y, et al. Psychosine-triggered endomitosis is modulated by membrane sphingolipids through regulation of phosphoinositide 4,5-bisphosphate production at the cleavage furrow. *Mol Biol Cell*. 2016;**27**: 2037-50.
40. Hein L, Meikle P, Hopwood J, et al. Secondary sphingolipid accumulation in a cell model of Gaucher disease. *Mol. Genet. Metab*. 2007;**92**:336-334.
41. Meikle P, Whitfield P, Rozaklis T, et al. Plasma lipids are altered in Gaucher disease: biochemical markers to evaluate therapeutic intervention. *Blood Cells Mol Dis*. 2008;**40**:420-7.

42. Alessandri G, De Cristan G, Ziche M, et al. Growth and motility of microvascular endothelium are modulated by the relative concentration of gangliosides in the medium. *J Cell Physiol*. 1992;**151**:23–28.
43. Slevin M, Kumar S, He X, et al. Physiological concentrations of gangliosides GM1, GM2 and GM3 differentially modify basic-fibroblast-growth-factor-induced mitogenesis and the associated signalling pathway in endothelial cells. *Int J Cancer*. 1999;**82**:412-23.
44. Lang Z, Guerrera M, Li R, et al. Ganglioside GD1a enhances VEGF-induced endothelial cell proliferation and migration. *Biochem Biophys Res Commun*. 2001;**282**:1031-7.
45. Birklé S, Zeng G, Gao L, et al. Role of tumor-associated gangliosides in cancer progression. *Biochimie*. 2003;**85**:455-63.
46. Berois N, Osinaga E. Glycobiology of neuroblastoma: impact on tumor behavior, prognosis, and therapeutic strategies. *Front Oncol.* 2014;**4**:114.
47. Chung T, Kim S, Choi H, et al. Ganglioside GM3 inhibits VEGF/VEGFR-2-mediated angiogenesis: direct interaction of GM3 with VEGFR-2. *Glycobiology*. 2009;**19**:229-
48. Seyfried T, Mukherjee P. Ganglioside GM3 Is Anti-angiogenic in Malignant Brain Cancer. *J Oncol*. 2010;**2010**:961243.
49. Suzuki K. Twenty Five Years of the "Psychosine Hypothesis": A Personal Perspective of its History and Present Status. *Neurochem Res.* 1998;**23**:251-259.

50. Wei Q, Zhang F, Richardson M, et al. CD82 restrains pathological angiogenesis by altering lipid raft clustering and CD44 trafficking in endothelial cells. *Circulation*. 2014;**130**:1493-504.
51. Margheri F, Papucci L, Schiavone N, et al. Differential uPAR recruitment in caveolar-lipid rafts by GM1 and GM3 gangliosides regulates endothelial progenitor cells angiogenesis. *J Cell Mol Med.* 2015;**19**:113-23.
52. Ziche M, Morbidelli L, Alessandri G, et al. Angiogenesis can be stimulated or repressed in vivo by a change in GM3:GD3 ganglioside ratio. *Lab Invest.* 1992;**67**:711-5.
53. Alessandri G, Cornaglia-Ferraris P, Gullino P. Angiogenic and angiostatic microenvironment in tumors--role of gangliosides. *Acta Oncol.* 1997;**36**:383-7.
54. Mukherjee P, Faber A, Shelton L, et al. Thematic review series: sphingolipids. Ganglioside GM3 suppresses the proangiogenic effects of vascular endothelial growth factor and ganglioside GD1a. *J Lipid Res*. 2008;**49**:929-38.
55. Koochekpour S, Merzak A, Pilkington G. Vascular endothelial growth factor production is stimulated by gangliosides and TGF-beta isoforms in human glioma cells in vitro. *Cancer Lett.* 1996;**102**:209-15.
56. Mandal C, Sarkar S, Chatterjee U, et al. Disialoganglioside GD3-synthase over expression inhibits survival and angiogenesis of pancreatic cancer cells through cell cycle arrest at S-phase and disruption of integrin-β1-mediated anchorage. *Int J Biochem Cell Biol.* 2014;**53**:162-73.

ACKNOWLEDGMENTS

Our thanks to Prof. Stefan Karlsson, University of Lund, Sweden, for providing his murine neuronopathic Gaucher animal model for use in these experiments; Dr. Sonoko Atsumi, Microbial Chemistry Research Foundation, Japan, for providing the cyclophellitol employed in these experiments; and Ms Hong Ngoc Thai, SA Pathology for technical assistance in preparation of tissues for the lipidomic analysis presented.

STATEMENT OF CONTRIBUTION

NJCS is responsible for the design, conduct and analysis of the experimental work presented, and the draft and revision of the final manuscript. JS and MF are responsible for generation and analysis of the lipidomic data presented, and contributed to review of the manuscript. TMC contributed to the design and analysis of the experiments presented, and review of the submitted manuscript.

FIGURES:

Figure 1. Mean vessel length volume density (L_{vd}) (µm x10^{-4}/µm^3) by anatomical subregion: Mean L_{vd} in wild type control (n = 3) and disease (n = 3) animals within the neocortex and thalamus [mean ± SEM & individual mean values displayed].

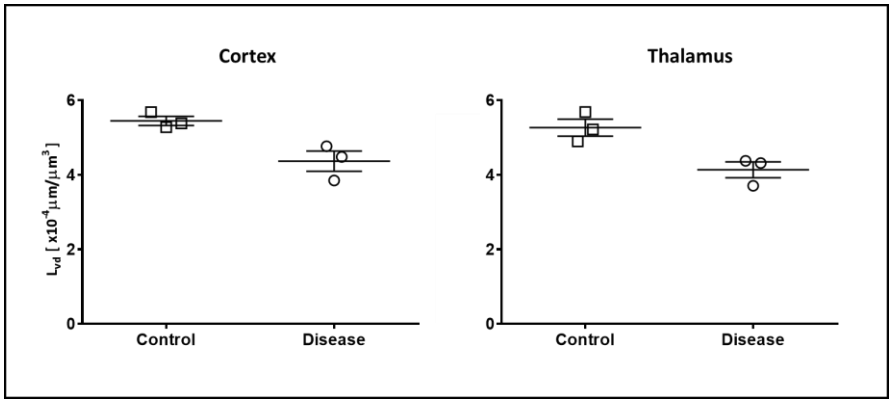

Figure 2. Sub-regional brain glucosylsphingosine (GluSph) and monohexosylceramide (MHC): Concentrations of GluSph are presented as mean ± SEM (A) and total MHC is expressed as the sum of the concentrations of seven acyl chain species as the mean ± SEM (B) in the cortex and sub-cortex. Open bars represent WT and filled bars nGD. **p <0.01; n=4.

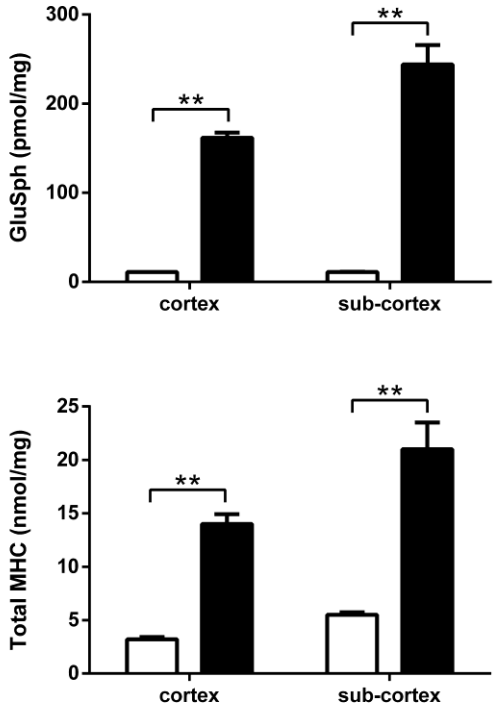

Figure 3. Sub-regional brain monosialated gangliosides G_{M1}, G_{M2} and G_{M3}: Total G_{M1} is expressed as a sum of the concentrations of d18:1/16:0, d18:1/18:0, d18:1/20:0 and d18:1/22:0, total G_{M2} and G_{M3} each a sum of d18:1/18:0 and d18:1/20:0 (see supplementary Table 1 for species measured). Results are expressed as the mean concentration ± SEM in the cortex and sub-cortex. Open bars represent WT and filled bars nGD. **p <0.01, *p <0.05; n=4.

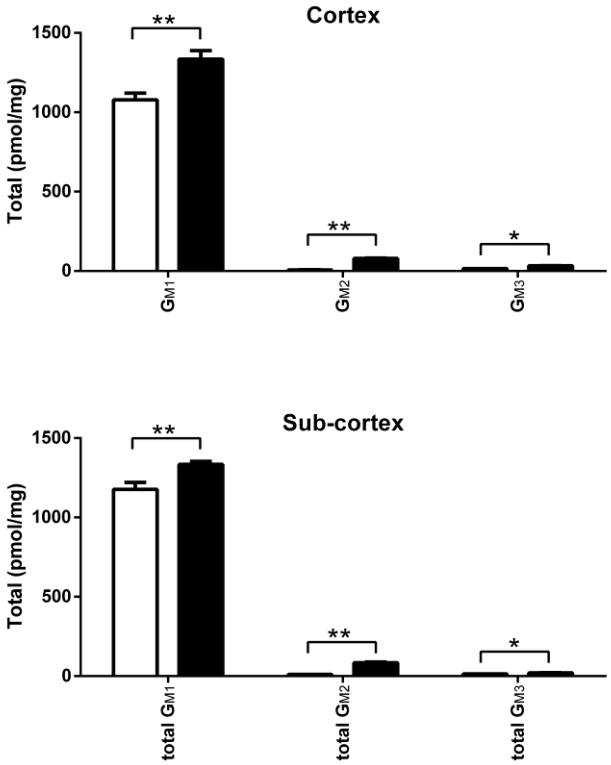

Figure 4. Species of G_{D1a} in the cortex and sub-cortex: Individual species of G_{D1a} are presented as the mean concentration ± SEM. Concentrations of d18:1/18:0 use the right hand y axis. Open bars represent WT and filled bars nGD. **p <0.01, *p <0.05; n=4.

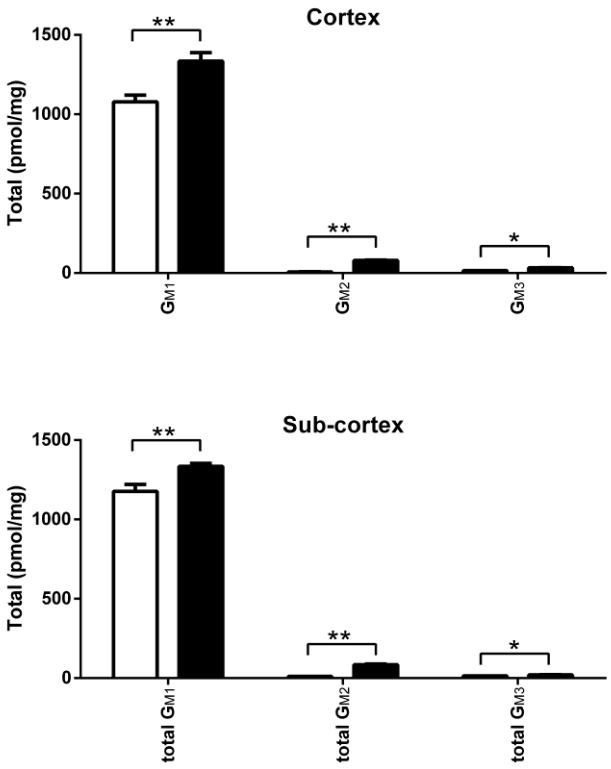

Figure 5. Species of G_{D2} and G_{D3} in the cortex and sub-cortex. Individual species of G_{D2} and G_{D3} are presented as the mean concentration ± SEM on the left hand and right hand y axis, respectively. Open bars represent WT and filled bars nGD. **p <0.01; n=4.

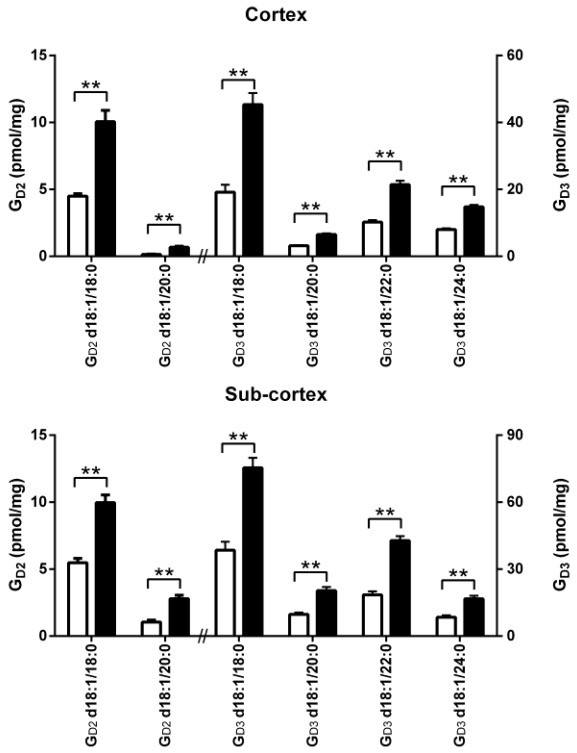

Table 1. Ganglioside relative concentrations

	'Anti-angiogenic'		'Pro-angiogenic'				
	GM3		GM1	GM2	GD1a	GD2	GD3
Cortex [control]	**1.0**	**:**	**59.8**	**0.6**	**149.0**	**0.3**	**1.6**
Cortex [Gaucher]	**1.0**	**:**	**30.8**	**2.8**	**86.1**	**0.4**	**1.7**
Subcortex [control]	**1.0**	**:**	**78.9**	**0.9**	**156.8**	**0.5**	**3.9**
Subcortex [Gaucher]	**1.0**	**:**	**55.9**	**4.6**	**88.1**	**0.6**	**4.7**
Cerebellum [control]	**1.0**	**:**	**38.6**	**0.8**	**59.6**	**0.5**	**11.0**
Cerebellum [Gaucher]	**1.0**	**:**	**29.6**	**3.2**	**43.3**	**0.7**	**10.9**

Relative concentrations normalised to GM3.

SUPPLEMENTARY FIGURES:

Supplementary Figure 1. Percentage multinucleated cells within glucosylsphingosine treated human umbilical vein endothelial cell monolayers: Mononucleated, binucleated and multinucleated mean percentage cell count, relative to glucosylsphingosine treatment concentration (0µM, 5µM, 10µM) at 24 hour and 48 hour time points.

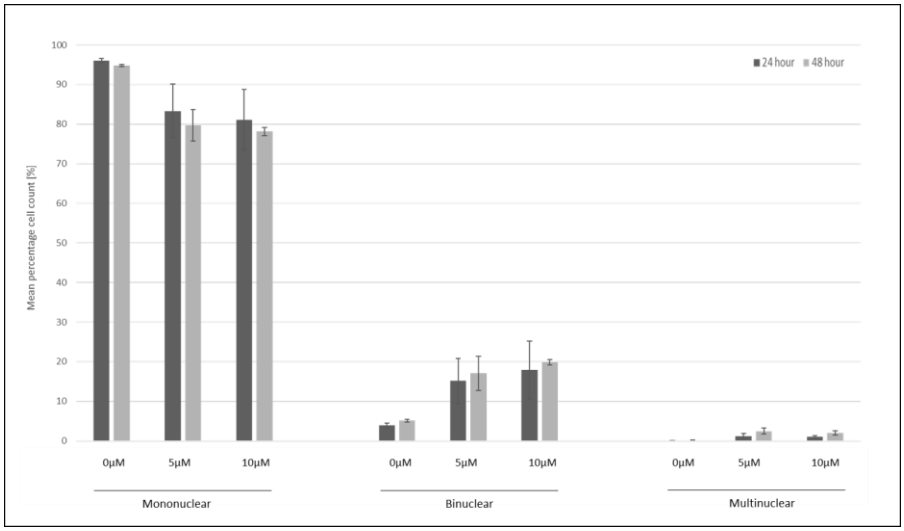

Supplementary Figure 2. Human umbilical vein endothelial cell monolayer wound closure assays: Percentage wound closure within glucosylsphingosine treated human umbilical vein endothelial cell (HUVEC) monolayers. (a) wound closure in β-glucocerebrosidase replete HUVEC monolayer and (b) wound closure in β-glucocerebrosidase inhibited (cyclphellitol treated) HUVEC monolayer. A concentration dependent retardation in wound closure was evident, irrespective of endogenous enzyme inhibition with cyclophellitol, upon treatment with escalating concentrations of glucosylsphingosine.

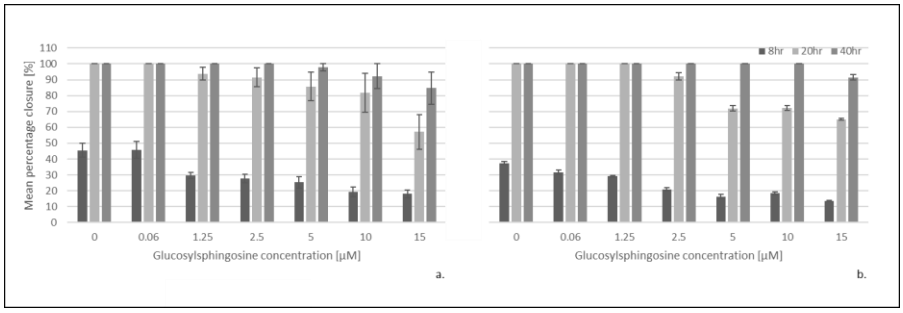

Supplementary Figure 3. Acyl chain species of monohexosylceramide (MHC) and dihexosylceramide (DHC): Individual acyl chain MHC and DHC species are presented as the mean concentration ± SEM in the cortex and sub-cortex. Open bars represent WT and filled bars nGD. **p <0.01, *p <0.05; n=4.